

RSC Advances



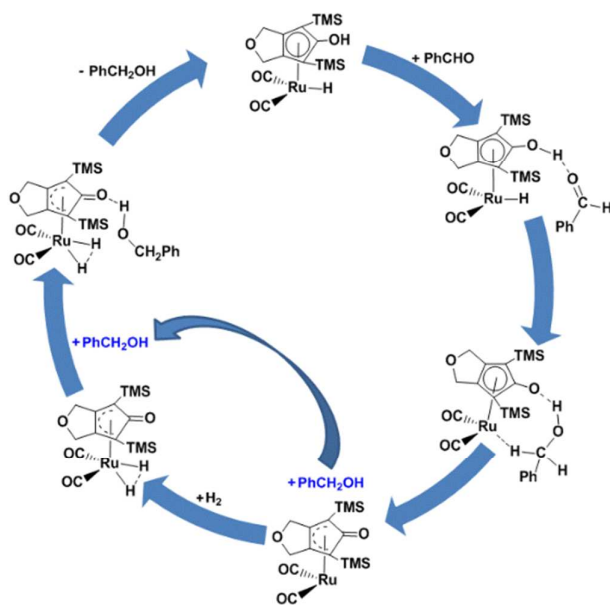
This is an *Accepted Manuscript*, which has been through the Royal Society of Chemistry peer review process and has been accepted for publication.

Accepted Manuscripts are published online shortly after acceptance, before technical editing, formatting and proof reading. Using this free service, authors can make their results available to the community, in citable form, before we publish the edited article. This *Accepted Manuscript* will be replaced by the edited, formatted and paginated article as soon as this is available.

You can find more information about *Accepted Manuscripts* in the [Information for Authors](#).

Please note that technical editing may introduce minor changes to the text and/or graphics, which may alter content. The journal's standard [Terms & Conditions](#) and the [Ethical guidelines](#) still apply. In no event shall the Royal Society of Chemistry be held responsible for any errors or omissions in this *Accepted Manuscript* or any consequences arising from the use of any information it contains.

The catalytic cycle of PhCHO hydrogenation catalyzed by Casey's Ru-complex:



Cite this: DOI: 10.1039/c0xx00000x

www.rsc.org/xxxxxx

ARTICLE TYPE

Density Functional Investigations on Catalytic Cycle of Hydrogenation of Aldehydes Catalyzed by an Enhanced Ruthenium Complex: An Alcohol-bridge Participated Autocatalysis Process

Xi Lu,^a Qian Liu,^a Xiaoyin Wang,^b Runjiao Cheng,^b Mingtao Zhang^{*b} and Xiaomin Sun^{*c}

Received (in XXX, XXX) Xth XXXXXXXXX 20XX, Accepted Xth XXXXXXXXX 20XX

DOI: 10.1039/b000000x

Abstract: A novel ruthenium complex developed by Casey exhibits some outstanding features such as effective anti-dimerization, highlighted catalytic activity and a mild reaction condition. Density functional theory (DFT) was used to explore the catalytic cycle of hydrogenation of PhCHO catalyzed by this enhanced ruthenium complex. The catalytic cycle of aldehyde hydrogenation involves two stages, hydrogen transfer and regeneration of active catalyst, which can be achieved by means of a concerted out-sphere hydrogen transfer and intramolecular hydrogen migration, respectively. The hydrogen transfer is the rate-determining step in the total catalytic hydrogenation cycle, corresponding to a low free energy barrier of 16.2 kcal/mol. The hydrogenated product, alcohol, can remarkably improve the regeneration activity of catalyst via an alcohol-mediated intramolecular hydrogen migration. The regeneration of active catalyst is only 13.8 kcal/mol here. This catalytic hydrogenation of aldehyde is demonstrated to be an autocatalysis process.

Introduction

Hydrogenation of aldehydes and ketones is an important transformation for synthesizing novel chemicals and expanding application of substrates.^{1,2} These carbonyl compounds are commonly reduced using the classic reagents such as LiAlH₄,³⁻⁵ which generally requires a strictly anhydrous condition and yields amount of metal-salt waste. Metal–ligand bifunctional catalysts⁶, by contrast, as a “green” surrogate has gradually replaced these stoichiometric reducing agents in the hydrogenation of polar double bonds. Transition-metal-catalyzed hydrogenation of aldehydes and ketones exhibits a higher catalytic activity indicating a lower cost and more economical benefits in industrial production.⁷ Furthermore, as hydrogen being a renewable resource, utilizing H₂ in organic synthesis is favorable to avoid causing the environmental pollution.⁸

Scheme 1. Shvo’s ligand-metal bifunctional complex.

Thereinto, Shvo’s catalyst^{9,10} discovered in the mid-1980s is a successful and famous ligand-metal bifunctional catalyst, [Ph₄(η⁵-C₄CO)Ru₂(CO)₄(μ-H) (scheme 1), which is popularly applied to hydrogen-transfer reactions of alkynes, carbonyls, and imines and

the oxidation of alcohols, amines, and other compounds.¹¹⁻¹⁷ Compound **A**, an air-stable and crystalline solid, itself can not catalyze hydrogen transfer of aldehydes and ketones. According to a kinetic study on the hydrogenation, Casey demonstrated that only generating the reduced **C** complex from dissociation of the diruthenium bridging hydride **A** under high H₂ pressure can achieve the catalytic hydrogenation. The oxidized **B** can be used to catalyze dehydrogenation reaction of alcohol and so on.^{18,19}

Scheme 2. Catalytic hydrogenation catalyzed by Knölker’s iron-catalyst **D**.

To further improve the catalysis of ruthenium complex, it is useful and applicably to understand the mechanisms for the use of Shvo’s catalyst. Since 2001, many experimental researches were performed to study the mechanism of hydrogenation and dehydrogenation reactions catalyzed by Shvo’s catalyst.^{18, 20-24} Until 2007, Casey proposed a concerted out-sphere hydrogen transfer mechanism based on the kinetics study for iron-complex catalyzed hydrogenation of aldehyde (Scheme 2).²⁵ However, due to the regeneration rate of catalyst being too rapid, he was not able to observe the detailed process of catalyst regeneration or perform a related study.

Scheme 3. The novel ruthenium complex **1** synthesized by Casey and Guan.

Based on the inspiration of Knölker's iron-catalyst **D**, a more active ruthenium catalyst **1**, [2,5-(SiMe₃)₂-3,4-(CH₂OCH₂)(η⁵-C₄COH)]Ru(CO)₂H, was successfully developed by Casey, which presented a significantly enhancement relative to Shvo's catalyst (scheme 3).²⁶ In addition, there is no bridging hydride formation for complex **1** in toluene. This ruthenium hydride can catalyze the the hydrogenation of both aldehydes and ketones under mild conditions (25 °C, 3 atm of H₂, scheme 4). Here, understanding the nature of this advanced ruthenium complex **1** is very helpful and useful to further find and develop other higher active ruthenium catalysts. Actually, Casey and Guan once intended to monitor the catalytic cycle, but they only observed the kinetic action on the hydrogen transfer of the catalytic hydrogenation between -68 and -54 °C under non-hydrogen environment as this hydrogenation rate being too rapid to follow at room temperature. However, a whole catalytic hydrogenation cycle should contain the regeneration of catalyst **1** beside the hydrogen transfer. Lacking of senses on catalyst regeneration is difficult to provide potent and cogent recommendations to the design of novel ruthenium catalysts and the modification of reaction conditions.

Scheme 4. Relative catalytic activity of hydrogenation of PhCHO in toluene at 25 °C under 3atm H₂ pressure obtained by Casey and Guan (the unreactive reaction of **C** is due to formed non-catalysis dimerization like **A** shown in scheme 1).

Since only depending on experimental techniques encountered a serious limitation, the theoretically chemical method is an appropriately supporting selection for investigating the totally catalytic hydrogenation of PhCHO. Previously, many reasonable explanations and results given by density functional method (DFT) on the mechanism of Shvo's and Knölker's catalyst catalyzed hydrogen transfer of both aldehydes and ketones are in well agreement with the experimental conclusions and observations.²⁷⁻²⁹ In this work, a deep and detailed computational research was performed on the elementary steps involved with Casey's modified ruthenium complex catalyzed aldehyde hydrogenation. The calculated results were expected to clarify relationships between structures and actions in order to supply functional and reliable information to experiment.

Computational details

Calculations for all geometries were carried out using the Gaussian 09 software package³⁰. Optimizations were performed at the density functional theory (DFT) level by means of the hybrid B3LYP³¹ functional and LACVP* basis set. The effective core potential LANL2DZ³² along with its associated basis set was employed for ruthenium and the main group elements (C, O, H, and Si) were calculated using the 6-31G* basis set. The structural parameters for ruthenium complex **1** that used in all calculations were obtained based on the X-ray crystal structure obtained by

Casey and Guan.²⁶ The entire aromatic ligand of ruthenium complexes is referred to as CpOH in this paper.

All calculations were done without any geometrical constraints. Frequency calculations were performed for all stationary points at the same level in order to identify the minima (zero imaginary frequency) and transition states (TS, only one imaginary frequency) and to provide free energies at 298.15 K and 1 atm. Intrinsic reaction coordinate (IRC)³³ analysis was carried out to confirm that all stationary states were smoothly connected to each other. Solvent effects (in toluene) were included using the SMD model^{34,35} with the M06 method (as implemented in Gaussian 09) by performing single-point calculations via the B3LYP-optimized geometries at the higher level of basis set, where the def2-TZVP³⁶ was employed for Ru and the 6-31++G** was used for main group elements. Zhao and Truhlar^{37,38} reported that the M06 method has a high accuracy for the calculation of the thermochemistry and kinetics of transition metals and main-group elements.

A correction term of 1.8943 kcal/mol must be added to the *G*(sol) calculations to convert the gas-phase standard free energies at a standard state of 1 atm to the appropriate standard state for a solution of 1 mol/L.^{39,40} Then, solvation free energies Δ*G*(sol) were used in order to consider both entropic and solvent effects.

Results and Discussion

This catalytic cycle mainly involves two processes for Casey's ruthenium complex catalyzed hydrogenation of aldehyde (scheme 5). The first stage is the hydrogen transfer from catalyst to substrate: **1** → **2** + PhCHO → **3** → **4** → **5** + PhCH₂OH → **6**. An outer-sphere concerted hydrogen transfer mechanism has been demonstrated to be both kinetically and thermodynamically reasonable pathway for this process according to previously experimental and theoretical studies. The second stage is the regeneration of active catalyst **2**: (i) **5** + H₂ → **2**, (ii) **5** + PhCH₂OH + H₂ → **8** → **2** + PhCH₂OH, (iii) **5** + PhCH₂OH → **6** + H₂ → **8** → **2** + PhCH₂OH or (iv) **5** + PhCH₂OH → **6** + H₂ → **2** + (PhCH₂OH)₂. To our best investigation, there is not any computational study on the regeneration of the active catalyst **2**. Based on hydrogenated products and intermediates, there are four possible means for the regeneration of the catalyst. Then the DFT method was adopted to make a detailed investigation for the total catalytic cycle.

Scheme 5. Possible routes of the catalytic cycle of PhCHO hydrogenation catalyzed by Casey's Ru-complex.

Hydrogen transfer process of PhCHO catalyzed by ruthenium complex. The initial geometry of Casey's ruthenium catalyst was optimized at the B3LYP/LACVP* level in the gas phase. Then the most stable conformation **1** was obtained (figure 1), which was in good agreement with X-ray crystal structure (Table S1 of Supporting Information). The benzaldehyde was used as the substrate in our calculations in order to approach to experimental conditions. It was found that **1** had a strong coordination interaction between the Cp ligand and the ruthenium, which improved the thermodynamic stabilization of **1** to a large extent. Figure 1 shows that the dihedral angle of the H-Ru bond

and the C-O(H) bond of the CpOH ligand is 94.3° in the **1** geometry. This indicated that these two bonds were nearly perpendicular to each other. However, the hydride ion of H-Ru bond and hydroxyl group bond located on opposite direction in **1**, which was unfavorable to the outer-sphere concerted hydrogen transfer.

Figure 1. Optimized structures for the hydrogen transfer of PhCHO catalyzed by **1**. Distances in Å. HRuCO(H) indicated the dihedral angle. All hydrogen atoms connected to carbons in the CpOH ring were ignored.

According to our previous computational studies on Knölker's catalyst²⁹, conformation **1** actually was a non-rigid structure in toluene and facilely transformed to the other isomer **2** via the transition state **1/2TS**. The dihedral angle of HRuCO(H) was reduced to 36.3° in **1/2TS**, which indicated that conformation **1** transformed to **2** by means of an intramolecular rotation of CpOH group. Figure 2 shows that the activation free energy $\Delta G^\ddagger(\text{sol})$ for this isomerization reaction is only 5.3 kcal/mol, which is a kinetically rapid step. In **2**, the HRuCO(H) dihedral angle was only -6.4°, indicating that the H-Ru and C-O(H) bonds became almost coplanar. Thus the H⁺...H distance in complex **2** was greatly shortened which was a more favorable structure for the transfer of two hydrogen atoms to the substrate. Besides, this step was also thermodynamically facile due to the $\Delta G(\text{sol})$ between **1** and **2** being only 1.2 kcal/mol. This presented that **1** \rightleftharpoons **2** was actually a fast equilibrium in toluene.

Figure 2. Free energy $\Delta G(\text{sol})$ profiles (kcal/mol) for the hydrogen transfer of PhCHO catalyzed by Ru-catalyst **1**. Relative to free energies of **1** and PhCHO.

In the next step, the free PhCHO in system bound to the active catalyst **2** via a hydrogen bond interaction and formed an intermediate **3** where the CpOH...OHCPH distance was 1.767 Å. Due to the effect of the entropic penalty, the thermodynamic stabilization of **3** was reduced to some extent. The reaction of **2** + PhCHO \rightarrow **3** was endergonic by 7.5 kcal/mol. This indicated that the intermediate **3** was thermodynamically unstable in the process of hydrogenation at room temperature, which was also in agreement with the experimental observation. In particular, this hydrogen bond effectively shrunk the distance between catalyst and substrate, which was more favorable to the hydrogen atom migrate from **2** to PhCHO.

Then the intermediate **3** transferred to another intermediate **4** through transition state **3/4TS** where the proton of the CpOH group and the hydride ion of the Ru-H bond concertedly added to the oxygen and carbon atoms of aldehyde group, respectively. The free energy barrier $\Delta G^\ddagger(\text{sol})$ was only 8.7 kcal/mol for the **3** \rightarrow **4** reaction, which was a kinetically facile step. In the geometry of **4**, the newly formed PhCH₂OH connected with the oxidized ruthenium complex via a hydrogen bonding which the CpO...HO distance was 1.761 Å and an agostic-H bonding interaction which the Ru...H distance was 2.016 Å. Due to ruthenium atom unachieved 18 electrons, the intermediate **4** was also

thermodynamically unstable, for which the $\Delta G(\text{sol})$ was increased to 7.8 kcal/mol compared with **1**.

The dissociation of **4** produced isolated ruthenium complex **5** and free PhCH₂OH. Due to **4** \rightarrow **5** + PhCH₂OH being entropically favorable, it was exergonic by 2.1 kcal/mol for this dissociation. But **5** also did not satisfy the 18-electronic structure of ruthenium. Then the free PhCH₂OH again connected to complex **5** using its hydroxyl group and obtained the complex **6** which was the final hydrogenated product without the presence of H₂. In product **6**, the oxygen atom of PhCH₂OH coordinated to the unsaturated ruthenium center in order to make it achieve 18-electronic structure; while the hydrogen atom of OH also formed a hydrogen bonding interaction with oxygen atom of CpO. So the reaction of **5** + PhCH₂OH \rightarrow **6** was exergonic by 3.0 kcal/mol.

However, **6** was not the most thermodynamically stable product in this hydrogenation, due to the $\Delta G(\text{sol})$ being 2.7 kcal/mol for **1** + PhCH₂OH \rightarrow **6**. This was also the reason that the crystal of **6** was not able to be obtained in experiments. But a similarly structural crystal was experimentally obtained for Knölker's iron-catalyst. Distances of Ru...O and CpO...HO-Bn were 2.304 and 1.805 Å in ruthenium complex **6**, respectively, which were longer than 2.069 and 1.734 Å of these bonds in the similar iron-complex geometry.²⁹ This meant that the coordination and hydrogen bonding interactions were reduced in ruthenium complex **6**. It was because the coordination bond between oxygen and 4d-orbital of ruthenium was to some extent receded by comparison to the bond between oxygen and 3d-orbital of iron.

In the catalytic cycle, the total free energy barrier was 16.2 kcal/mol for the hydrogen transfer from **2** to **6**, which consisted with Casey and Guan's experimental result of 15.3 kcal/mol. This was a kinetically facile process, so PhCHO was able to be hydrogenated with a very rapid rate under the catalysis of Casey's ruthenium catalyst at room temperature.¹⁸

The regeneration of active-catalyst 2. According to dehydrogenated product **5**, there are four possible pathways for the regeneration of the active-catalyst **2** under H₂ atmosphere. In route (i), H₂ is directly added to Ru-complex **5**, namely **5** + H₂ \rightarrow **7** \rightarrow **2**. In routes (ii) and (iii), the catalyst **2** is regenerated with the aid of an alcohol bridge only involving one PhCH₂OH molecule, which the detailed processes are **5** + H₂ \rightarrow **7** + PhCH₂OH \rightarrow **8** \rightarrow **2** + PhCH₂OH and **5** + PhCH₂OH \rightarrow **6** + H₂ \rightarrow **8** \rightarrow **2** + PhCH₂OH, respectively. In last route (iv), the regeneration of catalyst **2** is achieved via a double-alcohol bridge composed of a hydrogen bond, which the steps are **5** + H₂ \rightarrow **7** + (PhCH₂OH)₂ \rightarrow **9** \rightarrow **2** + (PhCH₂OH)₂.

Figure 3. Free energy $\Delta G(\text{sol})$ profiles (kcal/mol) for the regeneration route (i). Relative to free energies of **5** and H₂.

Actually, both regeneration routes (i) and (ii) start from H₂ adding to dehydrogenated Ru-complex **5**. Figure 3 shows that two σ -bond electrons of hydrogen coordinate to the unoccupied d-orbital of ruthenium through a transition state **5/7TS** in this step, which has an extremely small free energy barrier of 0.8 kcal/mol due to ruthenium center urgently demanding extra electrons to satisfy the 18 electrons structure. Then a stable dihydride intermediate **7** was obtained, where H-H formed a symmetric

coordination with Ru center due to both H \cdots Ru distances being 1.951 Å (figure 4). It was exergonic by 4.6 kcal/mol for **5** + H₂ → **7**.

Figure 4. Optimized structures for the route (i). Distances in Å.

For route (i), one coordinated hydrogen atom directly migrated to the carbonyl oxygen of CpO from Ru center in intermediate **7** via a transition state **7/2TS**, and then the catalyst **2** was regenerated. The reaction **7** → **2** was exergonic by 7.1 kcal/mol, but it had a high free energy of 29.8 kcal/mol which corresponded to a low reaction rate constant on kinetics. From **7/2TS**, the effectual distance was 1.374 Å for hydrogen migration to the carbonyl oxygen of the CpO group. However, both H \cdots O distances were 3.458 Å in the reactant **7** of this step. The coordinated H-H bond must twist to be vertical from horizontal in order to approach the carbonyl oxygen of CpO, whereas one hydrogen atom of H-H left from ruthenium during this twisting and its coordination interaction was to some extent reduced due to the H-Ru distance being 2.282 Å in **7/2TS**. In addition, the CpO group concertedly slipped towards the vertical hydrogen atom to further shrink the H \cdots O distance. These geometric adjustments were favorable to intramolecular hydrogen migration, but an overhigh strain was also created between CpO and ruthenium due to H-H strain. As a result, it led to a highly total free energy barrier of 25.2 kcal/mol in the route (i).

Figure 5. Free energy $\Delta G(\text{sol})$ profiles (kcal/mol) for the regeneration route (ii). Relative to free energies of **5**, H₂ and PhCH₂OH.

Compared with the route (i), the intramolecular hydrogen migration was achieved under the help of an alcohol bridge in the pathways (ii) and (iii) (figure 5). The difference between routes (ii) and (iii) was the generating means of a crucial intermediate **8**. For route (ii), the intermediate **7** firstly linked to a generated PhCH₂OH via a hydrogen bonding interaction, because the CpO \cdots HO-Bn distance was 1.810 Å in produced intermediate **8** (figure 6). Due to the entropic penalty of forming hydrogen bond, it was endergonic by 7.8 kcal/mol for **7** + PhCH₂OH → **8**. So it was totally endergonic by 3.2 kcal/mol for generating **8** by means of **5** + H₂ → **7** + PhCH₂OH → **8**.

Figure 6. Optimized structures for routes (ii) and (iii). Distances in Å.

Next, intermediate **8** occurred an intramolecular hydrogen migration with assistance of an alcohol-bridge. In transition state **8/2TS**, one hydrogen atom of H-H added to hydroxyl oxygen of PhCH₂OH and the hydroxyl hydrogen concertedly transferred to the carbonyl oxygen of the CpO group. Due to the participation of PhCH₂OH, the CpO \cdots H-H distance was enlarged to 2.806 Å compared with the directly transferring means via **7/2TS**, and it was only reduced by 0.652 Å relative to **7**. This indicated that the geometric tension during CpO, H-H and Ru-center was to a large

extent eased by an alcohol-mediated bridge. Besides, the closest distance between hydrogen of H-H and oxygen of PhCH₂OH was 2.676 Å in intermediate **8**, but it was shrunk to 1.302 Å in **8/2TS**. The shortened distance was 1.374 Å here, which is less than 2.084 Å between **7** and **7/2TS**. This meant the hydrogen atom was more facile to migrate to hydroxyl oxygen via **8**. Thus, the route (ii) corresponded to a lower total free energy barrier of 13.8 kcal/mol compared with the first route. The route (ii) was more kinetically favorable to implement the regeneration of **2** than the route (i).

Figure 7. Free energy $\Delta G(\text{sol})$ profiles (kcal/mol) for the regeneration route (iii). Relative to free energies of **5**, H₂ and PhCH₂OH.

Considering **6** being an alternative to intermediate **7**, there was the other means to generate intermediate **8**, namely **5** + PhCH₂OH → **6** + H₂ → **8** (figure 7). In the route (iii), **5** combined with a product PhCH₂OH prior to H₂ coordination and formed intermediate **6**. Then H₂ coordinated to ruthenium of **6** to replace the position of hydroxyl oxygen of alcohol. In the transition state **6/8TS** of this step, the CpO \cdots HO-Bn distance was 1.819 Å which meant hydrogen bonding interaction still existing; whereas the Ru \cdots OH was enlarged to 4.137 Å as the replacement of H₂ coordination (shown in figure 6). Due to the coordinated hydroxyl oxygen caused an obstruction for H₂ coordination, the free energy barrier was increased to 14.1 kcal/mol for **6** + H₂ → **8**. So the generating means of **8** in route (iii) corresponds to a total free energy barrier of 11.1 kcal/mol. The last step was the same as that of the route (ii). The total free energy barrier was also 13.8 kcal/mol for the route (iii). However, the barrier of **5** + H₂ → **7** + PhCH₂OH → **8** in route (ii) was 7.9 kcal/mol lower than that of **5** + PhCH₂OH → **6** + H₂ → **8** in route (iii). This presented that the former was much more kinetically favorable to produce intermediate **8**, so the route (ii) was more kinetically feasible compared with (iii).

Figure 8. Free energy $\Delta G(\text{sol})$ profiles (kcal/mol) for the regeneration route (iv). Relative to free energies of **5**, H₂ and PhCH₂OH.

It is well known that many intermolecular hydrogen bonds widely exist during alcohol molecules. This indicates that a long alcohol bridge involving two or more PhCH₂OH molecules can be formed via the intermolecular hydrogen bonding interactions. Since an alcohol-mediated bridge can effectively reduce the intramolecular geometric tension and authentically increase the regeneration activity of catalyst **2**, there is the other interesting issue whether or not a multiple-alcohol bridge can further improve the catalyst regeneration ability. Here a double-alcohol bridge was investigated firstly.

Figure 9. Optimized structures for the route (iv). Distances in Å.

As shown in figure 8, the first step of route (iv) is the same as that of route (ii), which is the process of H₂ adding to ruthenium, **5** +

H₂ → 7. From 7 to 9, a double-alcohol bridge bound to the carbonyl oxygen of CpO group via a hydrogen bonding interaction which the CpO...H distance corresponded to 1.745 Å (figure 9). From 9, the double-alcohol bridge established a looser geometry between ruthenium and CpO group, which the H-H...O was 2.075 Å. This structure was more favorable to hydrogen adding to hydroxyl oxygen atom. However, it was highly endergonic by 15.6 kcal/mol for 7 + (PhCH₂OH)₂ → 9. This was because two alcohol molecules simultaneously accessed to dihydride 7 caused a very high entropic penalty which exceeded the stabilization on structure performed by hydrogen bonds.

Then intermediate 9 transformed to catalyst 2 and free (PhCH₂OH)₂ through transition state 9/2TS with a free energy barrier of 9.6 kcal/mol. This barrier was 1.0 kcal/mol lower than that of 8 → 8/2TS → 2 + PhCH₂OH, which indicated that a double-alcohol bridge was more favorable to the intramolecular hydrogen migrating from ruthenium to carbonyl oxygen of CpO. This can be attributed to a long alcohol bridge created a looser geometry, the transition state 9/2TS, where the H-H...OCp distance was 3.509 Å very close to 3.458 Å of dihydride 7. So the hydrogen of H-H only needed a slightly movement and then it was able to add to hydroxyl oxygen of PhCH₂OH. Unexpectedly, the total free energy of the route (iv) was 20.6 kcal/mol, which was not further reduced compared with 13.8 kcal/mol of the route (ii). Thus, these facts presented that overhigh entropic penalties caused by a multiple-alcohol bridge were finally unfavorable to increase the regenerated activity of catalyst 2 relative to a single-alcohol bridge.

Completely catalytic cycle. As above analyses, the whole catalytic cycle for hydrogenation of PhCHO catalyzed by Casey's Ru-complex actually included two processes. Scheme 6 shows that the first stage is the hydrogen transfer, 1 → 2 + PhCHO → 3 → 4 → 5 + PhCH₂OH → 6, given birth to a total free energy barrier of 17.4 kcal/mol. Due to 2 + PhCHO → 3 merely being an endergonic reaction without any barrier, the concerted outer-sphere hydrogen transfer is the rate-determining step in this hydrogenation, namely 2 + PhCHO → 4. This corresponds to a free energy barrier of 16.2 kcal/mol.

Figure 10. The autocatalysis cycle of hydrogenation of benzaldehyde catalyzed by Casey's ruthenium complex 1 (kcal/mol).

The second stage is the regeneration of active catalyst 2, 5 + H₂ → 7 + PhCH₂OH → 8 → 2 + PhCH₂OH, possessed a total free energy barrier of 13.8 kcal/mol. The step of 7 + PhCH₂OH → 8 is also an endergonic reaction without barrier, so the intramolecular hydrogen migration from ruthenium to carbonyl oxygen of CpO group is the rate-determining step in this regeneration of catalyst 2, namely 7 + PhCH₂OH → 2. The free energy barrier is 18.4 kcal/mol, which is far higher than 0.8 kcal/mol of the addition reaction, 5 + H₂ → 7. This means the pressure of H₂ does not determine the regeneration rate of catalyst 2, which is in well agreement with Casey's experiments.²⁶

Compared with these two processes in catalytic cycle, the total free energy barrier of hydrogen transfer is 3.6 kcal/mol more than that of catalyst regeneration. So the hydrogen transfer is the rate-

determining step in the whole catalytic hydrogenation cycle. This indicates that the total free energy barrier for the catalytic cycle is 16.2 kcal/mol, which corresponds to a kinetically facile achievement. This is the reason that Casey's Ru-complex can catalyze hydrogenation of aldehydes in a mild reaction condition. However, the alcohol concentration is very low in an initial stage of hydrogenation. As a result, the factual reaction rate of regeneration is lower than that of hydrogen transfer, because the direct reduction from 5 to 2 corresponds to a higher free energy barrier of 25.2 kcal/mol in this case. Thus, if there is not extra alcohol added into toluene solution before reaction, the hydrogenation rate can be significantly increased after generated PhCH₂OH at the preliminary stage of catalytic cycle. These facts present that the catalytic hydrogenation of aldehydes is actually an autocatalysis process, because the generated alcohol can participate in the catalytic cycle and effectively decrease the free energy barrier of catalyst reactivation.

However, a comparison between regeneration route (ii) and (iv) presented that multiple-alcohol bridge can not further improve the regeneration activity of catalyst 2 relative to an alcohol-mediated bridge due to overhighly entropic penalties. This indicates that adding proper alcohol in reactive system is favorable to increase the hydrogenation rate, while this effect can not be further improved after the concentration of alcohol exceeding that of Ru-catalyst in solution. So the whole hydrogenation rate is mainly controlled by hydrogen transfer step when sufficient quantities of PhCH₂OH generated in catalytic cycle.

Conclusions

The catalytic cycle of Casey's Ru-complex catalyzed hydrogenation of PhCHO was studied using DFT method in detail. Solvation effects in toluene were also considered and were included in calculated free energy profiles. This catalytic cycle actually involves two stages: hydrogen transfer and regeneration of active catalyst 2. The hydrogenation of aldehydes can be implemented via a concerted out-sphere hydrogen transfer pathway. The regeneration of active catalyst 2 can be achieved by means of intramolecular hydrogen migration. Here an alcohol-mediated bridge displays a crucial function on enhancing the regeneration activity of catalyst 2.

This catalytic hydrogenation of aldehydes is actually an autocatalysis process. The hydrogen transfer is the rate determining step in the whole catalytic hydrogenation cycle. Besides, the intramolecular hydrogen migration is the rate-determining step in regeneration stage. These present that the pressure of H₂ does not determine the whole catalytic hydrogenation rate. Adding proper alcohol into toluene solution before reaction is favorable to significantly improve the regeneration activity of catalyst and then effectively enhance the catalytic hydrogenation rate. However, this function can not be further improved when the concentration of alcohol exceeds that of Ru-catalyst in solution.

Acknowledgement

This work is supported by National Natural Science Foundation of China (No. 21277082 and 21337001), Marie Curie International Research Staff Exchange Scheme Fellowship within

the 7th European Community Framework Programme (No. 295132) and Program for New Century Excellent Talents in University (NCET-13-0349).

Notes and references

^a Department of Chemical and Materials Engineering, University of Alberta, Edmonton, AB, T6G 2V4, Canada; E-mail: xlu2@ualberta.ca.

^b Computational Center for Molecular Science, College of Chemistry, Nankai University, Tianjin 300071, People's Republic of China; E-mail: zhangmt@nankai.edu.cn.

^c Environment Research Institute, Shandong University, Jinan, 250100, People's Republic of China; E-mail: sxmvch@sdu.edu.cn.

† Electronic Supplementary Information (ESI) available: [Total electronic energies, thermal corrections to Gibbs free energies and Cartesian coordinates, and so on]. See DOI:

Keywords: ruthenium complex; catalytic cycle; hydrogen transfer; regeneration of catalyst; hydrogenation.

1 H. U. Blaser, C. Malan, B. Pugin, F. Spindler, H. Steiner, M. Studer, *Adv. Synth. Catal.* 2003, **345**, 103–151.

2 P. N. Rylander in *Hydrogenation Methods*, Academic Press, New York, 1990.

3 B. M. Trost, I. Fleming in *Comprehensive organic synthesis: selectivity, strategy, and efficiency in modern organic chemistry*, 1st ed.; Pergamon Press: Oxford, England, 1991.

4 J. Seyden-Penne in *Reductions by the alumino- and borohydrides in organic synthesis*, 2nd ed.; Wiley-VCH: New York, 1997.

5 V. Fehring, R. Selke, *Angew. Chem. Int. Ed.* 1998, **37**, 1827–1830.

6 M. Yamakawa, H. Ito, R. Noyori, *J. Am. Chem. Soc.* 2000, **122**, 1466.

7 S. Enthaler, K. Junge, M. Beller in *Iron catalysis in organic chemistry: reaction and applications*, Wiley-VCH: Weinheim, 2008 and references therein.

8 (a) D. B. Levin, L. Pitt, M. Love, *Int. J. Hydrogen Energy* 2003, **29**, 173–185; (b) J. I. Hayashi, S. Hosokai, N. Sonoyama, *Process Saf. Environ. Prot.* 2006, **84**, 409–419; (c) A. J. Esswein, D. G. Nocera, *Chem. Rev.* 2007, **107**, 4022–4047; (d) A. Kudo, Y. Miseki, *Chem. Soc. Rev.* 2009, **38**, 253–278.

9 Y. Blum, D. Czarkie, Y. Rahamim, Y. Shvo, *Organometallics* 1985, **4**, 1459–1461.

10 Y. Shvo, D. Czarkie, Y. Rahamim, D. F. Chodosh, *J. Am. Chem. Soc.* 1986, **108**, 7400–7402.

11 (a) R. Karvemur, R. Prabhakaran, K. Natarajan, *Coord. Chem. Rev.* 2005, **249**, 911–918; (b) S. Gladiali, E. Alberico, *Chem. Soc. Rev.* 2006, **35**, 226–236.

12 Y. Shvo, I. Goldberg, D. Czierkie, D. Reshef, Z. Stein, *Organometallics* 1997, **16**, 133–138.

13 N. Menashe, E. Salant, Y. Shvo, *J. Organomet. Chem.* 1996, **514**, 97–102.

14 J. S. M. Samec, J. E. Bäckvall, *Chem. Eur. J.* 2002, **8**, 2955–2961.

15 J. S. M. Samec, A. H. Éll, J. E. Bäckvall, *Chem. Eur. J.* 2005, **11**, 2327–2334.

16 A. H. Éll, J. S. M. Samec, C. Brasse, J. E. Bäckvall, *Chem. Commun.* 2002, **10**, 1144–1145.

17 (a) A. L. E. Larsson, B. A. Persson, B. Pugin, J. E. Bäckvall, *Angew. Chem. Int. Ed.* 1997, **36**, 1211–1212; (b) B. A. Persson, A. L. E. Larsson, M. L. Ray, J. E. Bäckvall, *J. Am. Chem. Soc.* 1999, **121**, 1645–1650; (c) J. Paetzold, J. E. Bäckvall, *J. Am. Chem. Soc.* 2005, **127**, 17620–17621.

18 C. P. Casey, S. W. Singer, D. R. Powell, R. K. Hayashi, M. Kavana, *J. Am. Chem. Soc.* 2001, **123**, 1090–1100.

19 C. P. Casey, G. A. Bikzhanova, *Organometallics* 2002, **21**, 1955–1959.

20 L. S. M. Samec, J.-E. Bäckvall, P. G. Andersson, P. Brant, *Chem. Soc. Rev.* 2006, **35**, 237–248.

21 S. E. Clapham, A. Hadzovic, R. H. Morris, *Coord. Chem. Rev.* 2004, **248**, 2201–2237.

22 G. Csjernyk, A. H. Éll, L. Fadini, B. Pugin, J.-E. Bäckvall, *J. Org. Chem.* 2002, **67**, 1657–1662.

23 C. P. Casey, G. A. Bikzhanova, Q. Cui, I. A. Guzei, *J. Am. Chem. Soc.* 2005, **127**, 14062–14071.

24 J. B. Johnson, J.-E. Bäckvall, *J. Org. Chem.* 2003, **68**, 7681–7684.

25 C. P. Casey, H. Guan, *J. Am. Chem. Soc.* 2007, **129**, 5816–5817.

26 C. P. Casey, H. Guan, *Organometallics* 2012, **31**, 2631–2638.

27 A. Comas-Vives, G. Ujaque, A. Lledós, *Organometallics* 2007, **26**, 4135–4144.

28 H. Zhang, D. Chen, Y. Zhang, G. Zhang, J. Liu, *Dalton. Trans.* 2010, **39**, 1972–1978.

29 X. Lu, Y. Zhang, P. Yun, M. Zhang, T. Li, *Org. Biomol. Chem.* 2013, **11**, 5264–5277.

30 Gaussian 09 (Revision B.01), M. J. Frisch, G. W. Trucks, H. B.

31 Schlegel, G. E. Scuseria, M. A. Robb, J. R. Cheeseman, G. Scalmani, V. Barone, B. Mennucci, G. A. Petersson, H. Nakatsuji, M. Caricato, X. Li, H. P. Hratchian, A. F. Izmaylov, J. Bloino, G. Zheng, J. L.

32 Sonnenberg, M. Hada, M. Ehara, K. Toyota, R. Fukuda, J. Hasegawa, M. Ishida, T. Nakajima, Y. Honda, O. Kitao, H. Nakai, T.

33 Vreven, J. A. Montgomery, Jr. J. E. Peralta, F. Ogliaro, M. Bearpark, J. J. Heyd, E. Brothers, K. N. Kudin, V. N. Staroverov, R. Kobayashi,

34 J. Normand, K. Raghavachari, A. Rendell, J. C. Burant, S. S. Iyengar, J. Tomasi, M. Cossi, N. Rega, J. M. Millam, M. Klene, J. E.

35 Knox, J. B. Cross, V. Bakken, C. Adamo, J. Jaramillo, R. Gomperts, R. E. Stratmann, O. Yazyev, A. J. Austin, R. Cammi, C. Pomelli, J.

36 W. Ochterski, R. L. Martin, K. Morokuma, V. G. Zakrzewski, G. A. Voth, P. Salvador, J. J. Dannenberg, S. Dapprich, A. D. Daniels, O.

37 Farkas, J. B. Foresman, J. V. Ortiz, J. Cioslowski, D. J. Fox, Gaussian, Inc., Wallingford CT, 2009.

38 (a) A. D. Becke, *J. Chem. Phys.* 1993, **98**, 5648–5652; (b) C. Lee, W. Yang, R. G. Parr, *Phys. Rev. B* 1988, **37**, 785–789; (c) P. J. Stephens, F. J. Devlin, C. F. Chabalowski, M. J. Frisch *J. Phys. Chem.* 1994, **98**, 11623–11627.

39 P. J. Hay, W. R. Wadt, *J. Chem. Phys.* 1985, **82**, 270–283; *J. Chem. Phys.* 1985, **82**, 299–310.

40 (a) K. Fukui, *J. Phys. Chem.* 1970, **74**, 4161–4163; (b) K. Fukui, *Acc. Chem. Res.* 1981, **14**, 363–368.

41 A. V. Marenich, C. J. Cramer, D. G. Truhlar, *J. Phys. Chem. B* 2009, **113**, 4538–4543.

42 A. V. Marenich, C. J. Cramer, D. G. Truhlar, *J. Phys. Chem. B* 2009, **113**, 6378–6396.

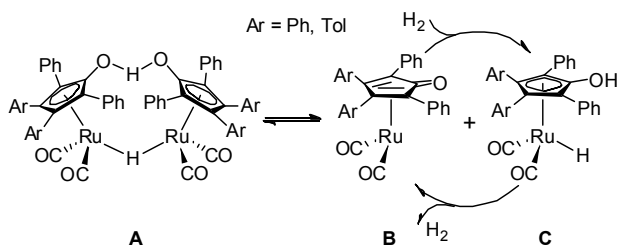
43 X. Xu, D. G. Truhlar, *J. Chem. Theory Comput.* 2012, **8**, 80–90.

44 Y. Zhao, D. G. Truhlar, *Acc. Chem. Res.* 2008, **41**, 157–167.

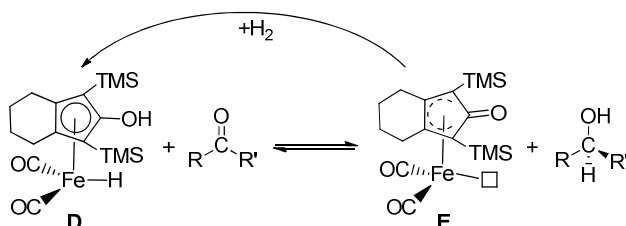
45 Y. Zhao, D. G. Truhlar, *Theor. Chem. Account.* 2008, **120**, 215–241.

46 L. M. Pratt, S. Merry, S. C. Nguyen, P. Quan, B. T. Thanh, *Tetrahedron* 2006, **62**, 10821–10828.

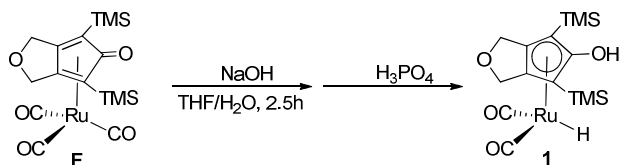
47 L. M. Pratt, D. G. Truhlar, C. J. Cramer, S. R. Kass, J. D. Thompson, J. D. Xidos, *J. Org. Chem.* 2007, **72**, 2962–2966.



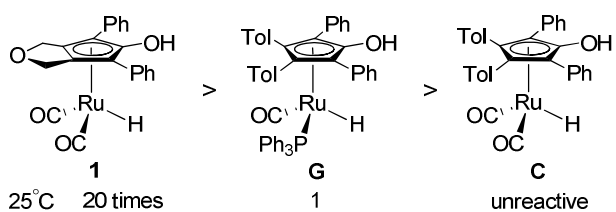
Scheme 1. Shvo's ligand-metal bifunctional complex.



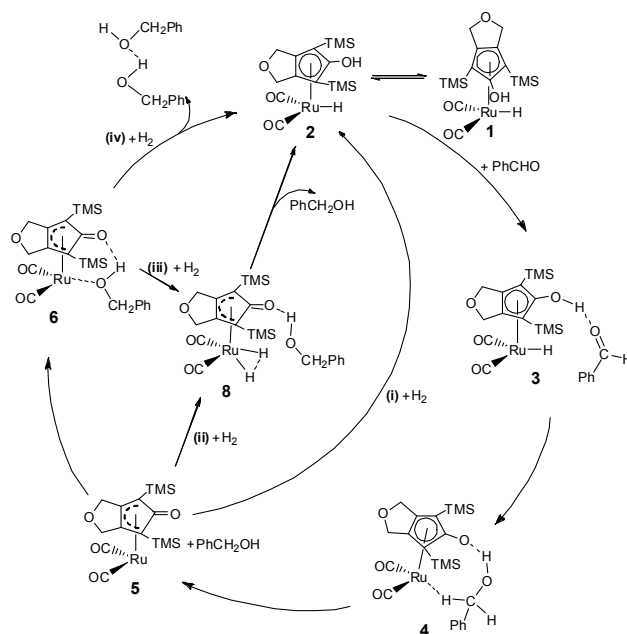
Scheme 2. Catalytic hydrogenation catalyzed by Knölker's iron-catalyst **D**.



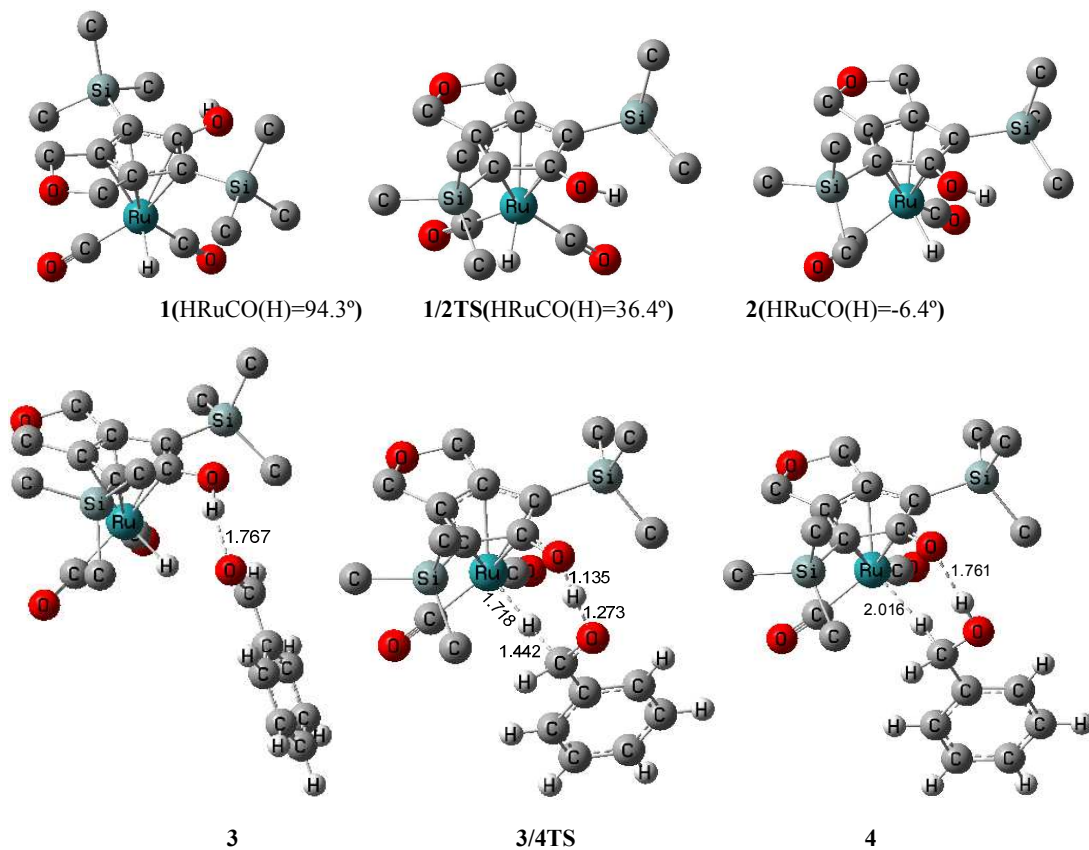
Scheme 3. The novel ruthenium complex **1** synthesized by Casey and Guan.



Scheme 4. Relative catalytic activity of hydrogenation of PhCHO in toluene at 25 °C under 3atm H₂ pressure obtained by Casey and Guan (the unreactive reaction of **C** is due to formed non-catalysis dimerization like **A** shown in scheme 1).



Scheme 5. Possible routes of the catalytic cycle of PhCHO hydrogenation catalyzed by Casey's Ru-complex.



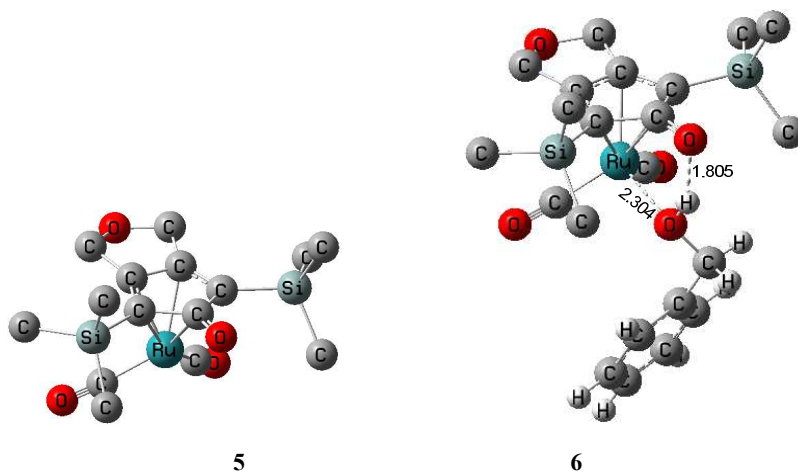


Fig. 1 Optimized geometries for 2i'TS and 2j'TS. Distances in Å. Optimized structures for the hydrogen transfer of PhCHO catalyzed by **1**. Distances in Å. HRuCO(H) indicated the dihedral angle. All hydrogen atoms connected to carbons in the CpOH ring were ignored.

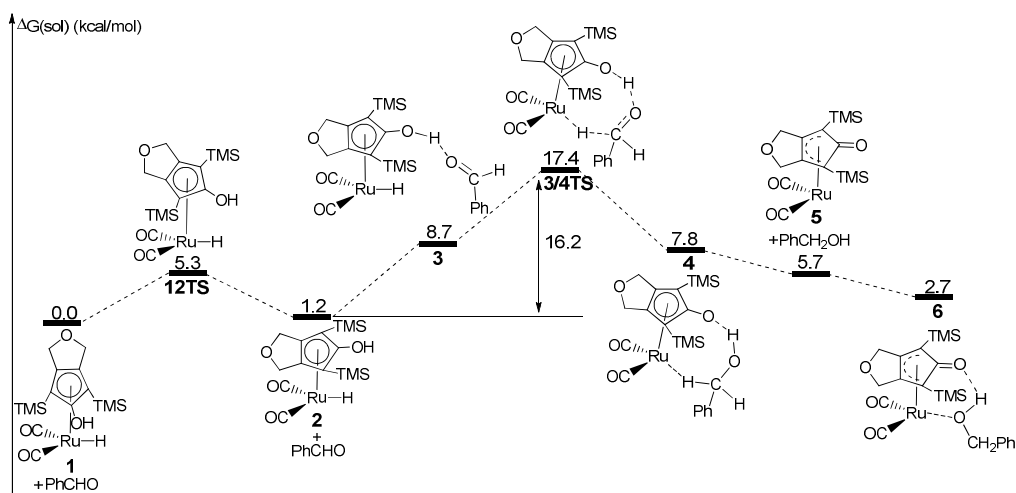


Fig. 2 Free energy $\Delta G(\text{sol})$ profiles (kcal/mol) for the hydrogen transfer of PhCHO catalyzed by Ru-catalyst **1**. Relative to free energies of **1** and PhCHO.

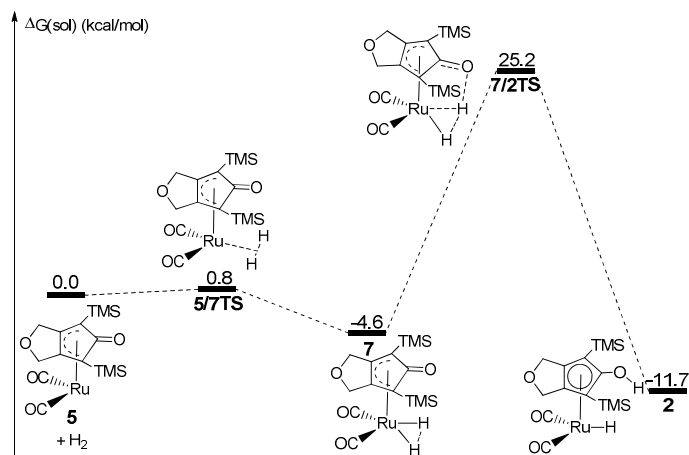


Fig. 3 Free energy $\Delta G(\text{sol})$ profiles (kcal/mol) for the regeneration route (i). Relative to free energies of **5** and H_2 .

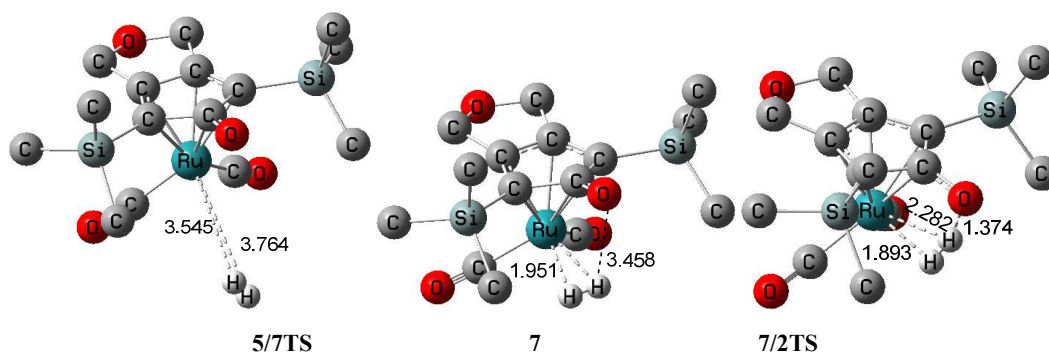


Fig. 4 Optimized structures for the route (i). Distances in Å.

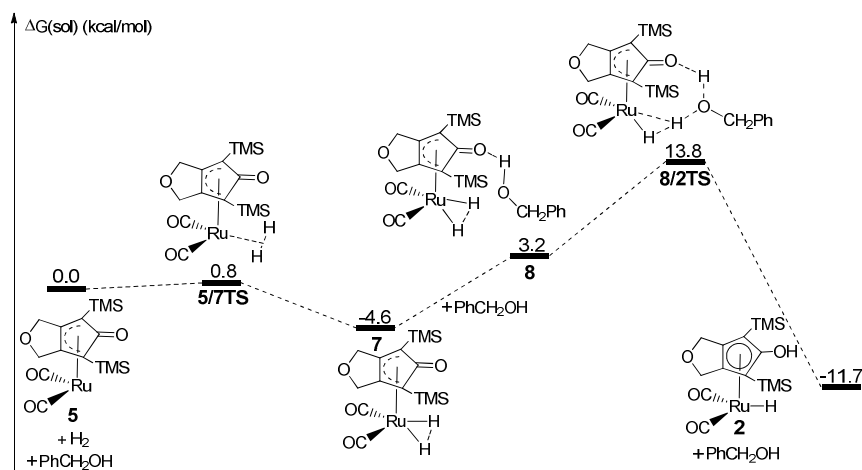


Fig. 5 Free energy $\Delta G(\text{sol})$ profiles (kcal/mol) for the regeneration route (ii). Relative to free energies of **5**, H_2 and PhCH_2OH .

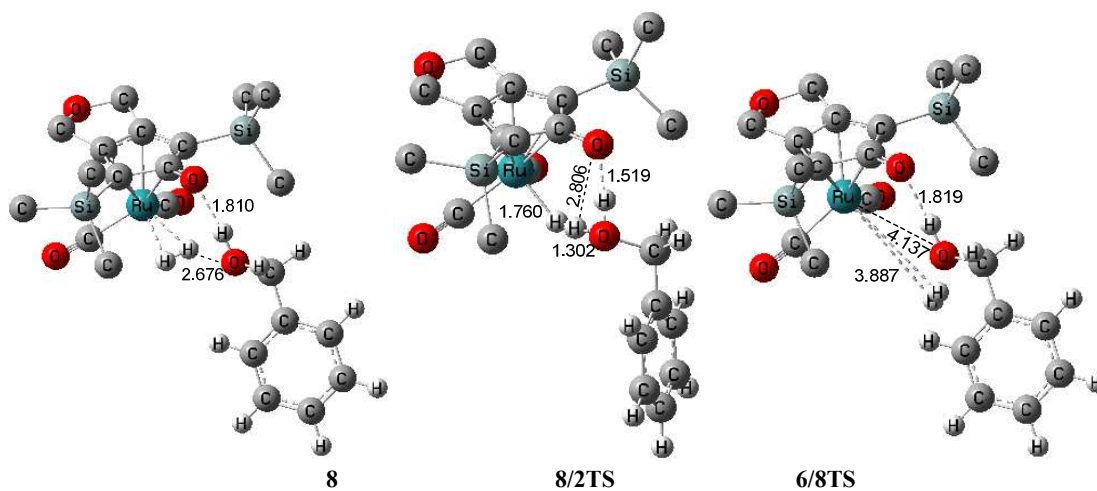


Fig. 6 Optimized structures for routes (ii) and (iii). Distances in Å.

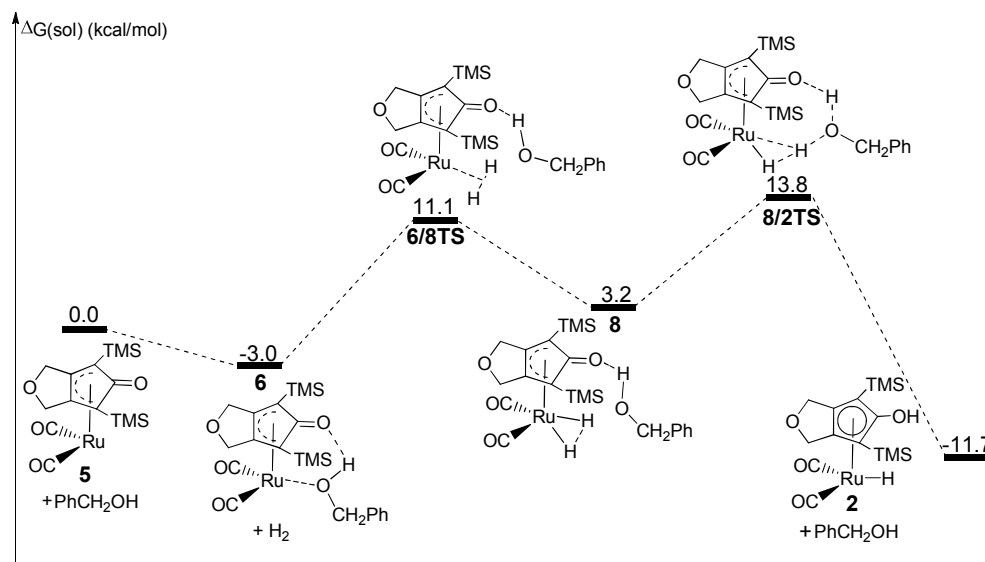


Fig. 7 Free energy $\Delta G(\text{sol})$ profiles (kcal/mol) for the regeneration route (iii). Relative to free energies of **5**, H_2 and PhCH_2OH .

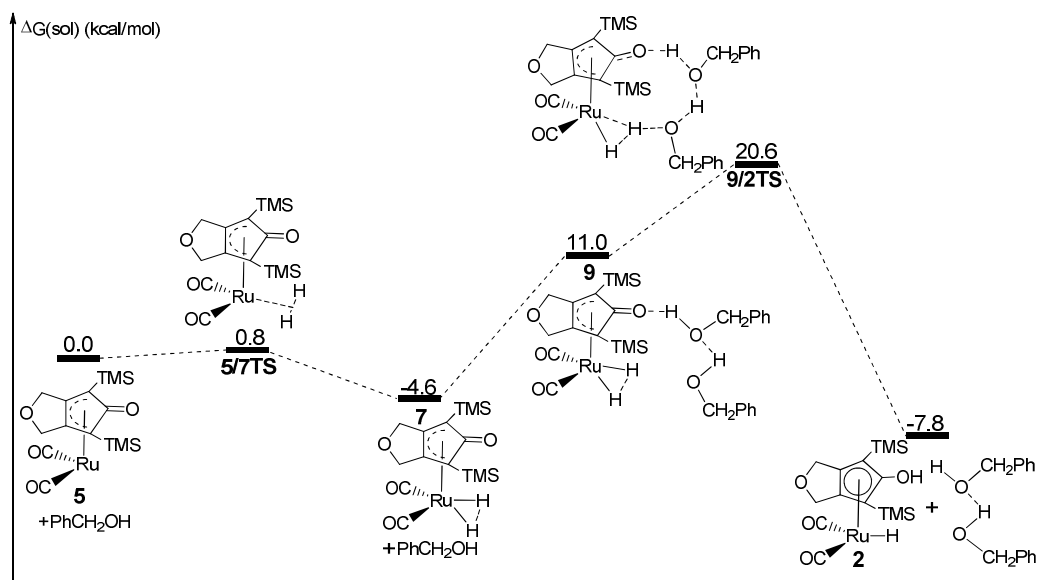


Fig. 8 Free energy $\Delta G(\text{sol})$ profiles (kcal/mol) for the regeneration route (iv). Relative to free energies of **5**, H₂ and PhCH₂OH.

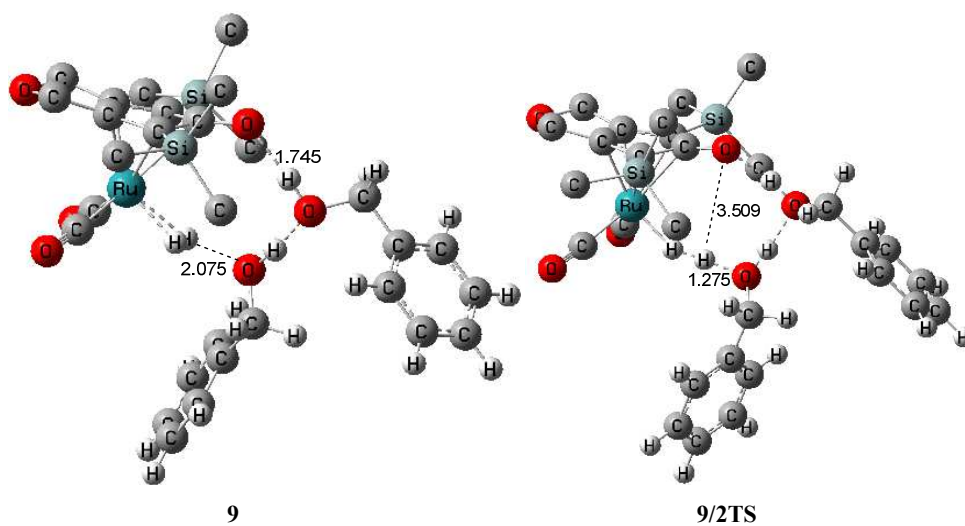


Fig. 9 Optimized structures for the route (iv). Distances in Å.

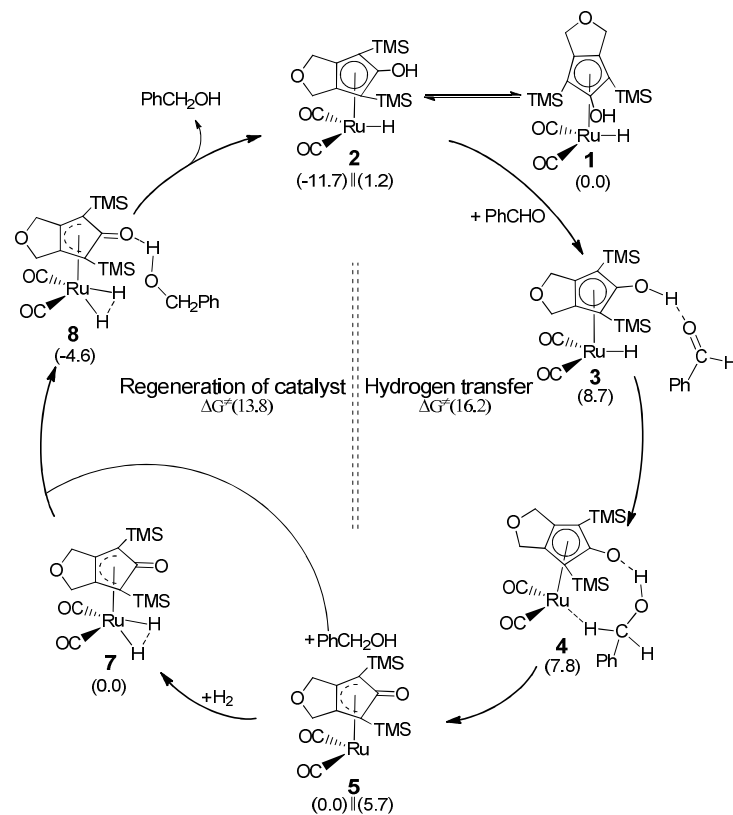


Fig. 10 The autocatalysis cycle of hydrogenation of benzaldehyde catalyzed by Casey's ruthenium complex **1** (kcal/mol).